

MODELING THE CHANGE OF BEACH PROFILE UNDER TSUNAMI WAVES: A COMPARISON OF SELECTED SEDIMENT TRANSPORT MODELS

LINLIN LI

Earth Observatory of Singapore, Nanyang Technological University, 50 Nanyang Avenue, 639798, Singapore

ZHENHUA HUANG*

Earth Observatory of Singapore and School of Civil and Environmental Engineering, Nanyang Technological University, 50 Nanyang Avenue, 639798, Singapore

Abstract: In contrast to the efforts made to develop hydrodynamic models for large-scale tsunami propagation and run-up, little has been done to develop, test and validate sediment transport models used to simulate tsunami-induced sediment movement. In this study, the performances of six widely-used sediment transport formulas are evaluated through case studies using an open source code XBeach, which is based on 2D depth-averaged nonlinear shallow water equations. Another open source code, Delft3D, is also used to see to what extent XBeach can give reliable results. The benchmarks used for case studies include three laboratory experiments and one field observation from a post-tsunami field survey conducted after the 2004 Indian tsunami. Our results show that most of the surveyed sediment transport formulas can give good results for laboratory-scale problems, but for real-scale problems, all six formulas failed to produce good results compared to those found in laboratory conditions. For laboratory-scale problems, both XBeach and Delft3D can predict satisfactory results with properly-chosen model parameters. For real tsunamis, high suspended sediment concentration may occur, and density stratification and hindered settling effect play an important role; therefore, Delft3D, with both hindered settling and density stratification being considered, may perform better than XBeach. The findings reported here will be useful for researchers and practitioners working on tsunami hazard mitigation.

Keywords: tsunami waves; sediment transport; model comparison

1. Introduction

Tsunami waves can cause widespread and dramatic changes in coastal morphology. Compared with storm waves or swells, tsunami waves have extremely long wavelength (10km~500km), long wave period (100s~2000s),

*Corresponding author email: zhhuang@ntu.edu.sg

and deep flow depth (up to 30 m or more). The velocity of tsunami flows could reach 10m/s or even higher near the shoreline[Goto *et al.*, 2007], which might cause high bed shear stresses with the Shields number being on the order of 10 [Paris *et al.*, 2010]. Due to the infrequent nature of tsunamis and the difficulty in conducting timely measurements after tsunami events, sediment transport is less understood compared to other tsunami characteristics.

Investigating the sediment movement induced by tsunamis is not only important for predicting potential tsunami hazards in the future, but also plays an important role in understanding the tsunami hazards which have occurred in the past. By analyzing tsunami deposits left by paleo-tsunamis or modern tsunamis, information on the number of attacking waves, flow depth and velocity may be inferred from the characteristics of deposited sediment such as mean grain size, sand size distribution, and deposit thickness[Jaffe and Gelfenbuam, 2007; Moore *et al.*, 2007; Spiske *et al.*, 2010]. This information can potentially help to reconstruct tsunami flow characteristics, assess tsunami source locations and estimate the recurrence intervals of past tsunamis [Martin *et al.*, 2008; Nelson *et al.*, 2006; Pinegina *et al.*, 2003; Switzer *et al.*, 2012]. However, this type of inverse interpretation relies crucially on a good understanding of how coastal sediment is transported and deposited by tsunamis, and thus poses a great challenge to the traditional methods used by tsunami geologists because tsunami deposits are highly variable and affected strongly by local conditions such as the tsunami waveform, coastal morphology, inland topography, composition and availability of sediment. Forward numerical models are particularly suitable for tackling issues of high uncertainty and complexity. Some open-source hydrodynamic codes for modeling tsunami propagation and inundation have been widely used in the past, including MOST [Titov and Synolakis, 1998], TUNAMI N2 [Goto *et al.*, 1998] and COMCOT [Liu *et al.*, 1995; Megawati *et al.*, 2009; Wang, 2009], and several benchmark cases have been developed at the International Workshops on Long-Wave Run-up for validating hydrodynamic models[Liu *et al.*, 2008; Yeh *et al.*, 1996]. Contrasting with the efforts made to develop and validate the hydrodynamic models, few attempts have been made to develop and validate the sediment transport models used to simulate the sediment movement induced by tsunamis.

Tsunami-induced sediment transport has been studied by several authors using various numerical models [Apotsos *et al.*, 2011a; Apotsos *et al.*, 2011c; Goto and Imamura, 2007; Li *et al.*, 2012b; Nakamura *et al.*, 2009; Simpson and Castellort, 2006; Sugawara *et al.*, 2004; Takahashi *et al.*, 2000; Xiao *et al.*, 2010], and these models can be roughly grouped into two categories: 2-dimensional models using depth-averaged shallow water equations [Li *et al.*, 2012b; Nishihata *et al.*, 2006; Simpson and Castellort, 2006] and 3-dimensional models [Apotsos *et al.*, 2011a; Apotsos *et al.*, 2011c; Nakamura *et al.*, 2009]. Both 2D and 3D models have their merits and drawbacks. 2D models are more efficient and suitable for simulating large-scale problems. However, since the vertical distribution of velocity and sediment concentration cannot be resolved in depth-averaged models, some important phenomena such as density stratification and hindered-settling effect cannot be discussed by 2D models. In this regard, 3D models have advantages over 2D models. However, running 3D models is computationally expensive, which limits 3D models to only small-scale problems. When modeling tsunami-induced sediment transport, empirical formulas are usually used together with either 2D or 3D models to quantify the incipient sediment motion and the equilibrium concentration of sediment in suspension. Since these empirical formulas were originally developed for river

engineering problems and most of them were calibrated only for low flow velocities and low sediment concentrations, it is desirable to assess the suitability of these empirical formulas for tsunami-induced sediment transport.

In this study, two widely-used open source codes (XBeach and Delft3D) are chosen to assess the suitability of six empirical formulas for tsunami-induced sediment transport. XBeach is a 2DH numerical model, which solves depth-averaged nonlinear shallow water equations (NLSWEs) in two dimensions; Delft3D solves a multi-layered system of NLSWEs in three dimensions. Our main objectives are to: (1) compare and discuss the appropriateness of using existing sediment transport formulas for tsunami-induced sediment transport, (2) evaluate the performance of XBeach and Delft3D in simulating morphological changes induced by tsunamis; (3) examine the sensitivity of XBeach and Delft3D to bottom friction, eddy viscosity and diffusivity, etc. The datasets used in this study include three sets of laboratory experimental results and one field observation at Kuala Meurisi, Sumatra, after the 26 December 2004 Indian Ocean tsunami.

2. XBeach and Delft3D

XBeach can simulate both storm waves and time-varying currents. The sediment movement is simulated by the depth-averaged advection-diffusion equation with a source term formulated by an equilibrium sediment concentration [Galappatti and Vreugdenhil, 1985]. The equilibrium sediment concentration can be calculated with various sediment transport formulas. The hydrodynamic performance of XBeach has been tested with several analytical solutions, large-scale laboratory experiments, and several field observations [Deltares, 2010; Li *et al.*, 2012b; McCall *et al.*, 2010; Roelvink *et al.*, 2009]. A detailed description of XBeach can be found in Roelvink *et al.* [2009].

Delft3D solves a multi-layered system of NLSWEs in three dimensions in a σ – coordinate system with the hydrostatic and Boussinesq assumptions [Lesser *et al.*, 2004]. The system of equations in the σ – coordinate system includes momentum equations, continuity equation, sediment transport equation, and turbulence closure models. In Delft3D, the suspended sediment transport is calculated by solving a three-dimensional advection-diffusion equation and the bed load is calculated using the sediment transport formula of Van Rijn [1993]. The elevation of the bed is dynamically updated at each computational time-step. A detailed description of Delft3D can be found in the user manual [Deltares, 2011].

Both XBeach and Delft3D employ eddy viscosity and diffusivity to determine the Reynold's stresses and turbulent diffusion, respectively. XBeach needs only the viscosity and diffusivity in the horizontal direction, while Delft3D needs both the vertical and horizontal viscosities and diffusivities. Both the values of eddy viscosity and diffusivity are affected by the turbulence length scale and grid size used in numerical simulations. In XBeach, the horizontal diffusivity accounts not only for turbulence transport but also the dispersive transport due to vertical non-uniformity in velocity [Rodi, 1984]. In Delft3D, both the horizontal viscosity/diffusivity includes two parts: the eddy viscosity/diffusivity computed by a 3D turbulence closure model and a user-defined background value used to

account for other non-resolved mechanisms. Therefore, both the horizontal diffusivity and viscosity used in XBeach represent slightly different physics from those used in Delft3D.

When a large amount of sediment is suspended from the sea bed, a stably-stratified water column exists near the bed, which may inhibit near-bed turbulence and the mixing of sediment into the upper water column. In Delft3D, density stratification is inherently accounted for in the $k-\varepsilon$ turbulence model by using the mixture fluid density. The settling velocity of a particle can also be significantly reduced when the suspended sediment concentration (hereafter we refer “suspended sediment concentration” as SSC) increase to a high level [van Rijn, 2007]. The hindered-settling effect will be more profound near the bottom where the sediment concentration is high.

3. Performance of existing sediment transport formulas for tsunami-like waves and real tsunamis

The suitability of some selected sediment transport formulas for the sediment movement induced by tsunamis is discussed in this section using XBeach. Sediment transport formulas examined in this study are summarized in Table 1; these formulas were proposed by Bagnold [1966], Engelund and Hansen [1967], Bijker [1967], Ackers and White [1973], Yang [1979] and Van Rijn [1984a; b]. According to the concept of energy balance, Bagnold [1966] related the transport of bed load and suspended load to the stream power of fluid. Along the line of Bagnold [1966], Engelund and Hansen [1967], Ackers and White [1973] analyzed a large amount of experimental data and developed their sediment transport formulas. The formula of Bijker [1967] originated from Einstein [1950], who assumed a rouse profile for the concentration and a logarithmic distribution of fluid velocity. Van Rijn [1993] proposed his formula for the sediment transport rate in rivers by using the approach of Bagnold for computing the bed load and integrating the product of the vertical concentration and velocity profiles over the flow depth for suspended load. Further details regarding these formulas can be found in most of the textbooks on sediment transport. For later discussion, the ranges of some key parameters in the datasets used to validate the sediment transport formulas are summarized in Table 2.

We present, in the rest of this section, comparisons between experimental/observational results with those simulated using the six formulas listed in Table 1. In all the simulations, the values of the model parameters were taken from the literature without any calibration. The four sets of data used for model evaluation are listed in Table 3: the first three are based on laboratory experiments using breaking solitary waves as proxies for tsunami waves and the last one is a field observation near Kuala Meurisi, Sumatra, after the 2004 Indian Ocean tsunami [Apotsos *et al.*, 2011a]. Table 3 also includes the information on the wave-flume dimensions, the median grain size (D_{50}), the water depth (h), the wave height (H), and the numbers of solitary waves (N) used in the experiments: Key parameters used in XBeach simulations, including the grid size Δx , the Chezy coefficient C , the eddy viscosity ν_h , and the diffusivity D_h , are also listed in Table 3 for reference. The values of D_h and ν_h were obtained based on a trial-and-error for each test case so that satisfactory results were obtained for all formulas (the sensitivity of the simulation results to the values of D_h and ν_h is discussed in Section 5). To compare with the field observation listed in Table 3, XBeach is implemented in a near-shore region, with incoming tsunami waves being specified on the offshore boundary;

weakly reflective boundary conditions(see, e.g., Van Dongeren and Svendsen [1997]) are imposed on other open boundaries so that outgoing waves can leave an open boundary with a minimum reflection.

3.1. *The experiment of Kobayashi and Lawrence (2004)*

Fig. 1 shows a comparison between the measured bed profile and those computed using different sediment-transport formulas. The results obtained using the formulas of Bagnold [1966], Ackers and White [1973] and Van Rijn [1984a; b] match remarkably well with the experimental results, especially in the erosion region. In contrast, the results obtained using the formulas of Engelund and Hansen [1967], Bijker [1967] and Yang [1979] show considerable underestimation in the erosion depth and deposition thickness. For the position of the maximum erosion, a noticeable difference exists between the measurement and the simulation obtained using the formula of either Bijker [1967] or Yang [1979].

3.2. *The experiment of Young et al (2010) for the solitary wave of height 0.3 m*

Fig. 2 shows a comparison between the measured changes of the bed profile and those computed using different sediment-transport formulas. In general, the formulas of Bagnold [1966] and Van Rijn [1984a; b] yield equally-good predictions, except that some overestimation of the erosion in the offshore area was found in the simulations. However, the formulas of Ackers and White [1973] and Engelund and Hansen [1967] underestimated the erosion depth and the deposition thickness. It is also noted that the formulas of Bijker [1967] and Yang [1979] failed to predict the correct location of the erosion region and that the deposition thickness was significantly underestimated by both formulas.

3.3. *The experiments of Young et al (2010) for the solitary wave of height 0.6 m*

Fig. 3 compares the measured changes of the bed profile with those computed using different sediment-transport formulas. The formulas of Bagnold [1966] and Van Rijn [1984a; b] gave the results in good agreement with the measurement, except that the erosion depth in the further inland area were overestimated by both formulas. The formula of Ackers and White [1973] also gave satisfactory results, except for an underestimation of the deposition thickness in the offshore region. The formula of Engelund and Hansen [1967] predicted the correct trends of the erosion and deposition distributions, but significantly underestimated both the erosion depth and the deposition thickness. Again, the formulas of Bijker [1967] and Yang [1979] failed to predict the correct location of erosion and significantly underestimated the deposition thickness.

3.4. *Kuala Meurisi, Sumatra*

The laboratory experiments discussed in Section 3.1 to 3.3 involved only solitary waves, whose scales can be quite different from those of real tsunamis [Apotsos *et al.*, 2011b]. Here we attempt to evaluate the sediment-transport formulas using the data collected from a post-tsunami field survey at Kuala Meurisi, northwest coast of Northern Sumatra, after the 2004 Indian Ocean Tsunami [Jaffe *et al.*, 2006]. The eroded beach profile was digitized from Figure 1 of Apotsos *et al.* [2011a], which also provided data for the cross-shore bathymetry (extending offshore to a water depth of 17 m) and the topography at Kuala Meurisi, Sumatra, as shown in Fig. 4(a). The rupture model and the tsunami waves propagating into the computational domain are the same as those used in Apotsos *et*

al. [2011a]. Fig. 4(b) shows the incident wave (digitized from Figure 3 of Apotsos et al. [2011a]), which consists of two large wave peaks (about 5 m high) and a series of smaller non-uniform waves. In the simulations, the waves are assumed to be normal to the shoreline, as did in Apotsos et al. [2011a]. The detailed model setup is summarized in Table 3.

Before we compare the measured deposit thicknesses along a cross-shore section with those computed using the 6 formulas, it is worth distinguishing the thickness of a deposition region from deposit thickness. In this paper, the thickness of a deposition region is defined as the tsunami-induced increase of the bed elevation from the original bed elevation (Fig. 5a). The thickness of a deposition region can be easily calculated in numerical simulations by comparing the pre- and post- event topographical data in the region; however, the thickness of a deposition region is difficult to obtain from field surveys unless pre-tsunami topography of the study area is available. In post-tsunami surveys, the deposit thickness (i.e., the thickness of the sediment deposited in an area) is usually measured. We stress that the final bed elevation in the area where the deposit thickness is measured can be lower than the corresponding pre-tsunami elevation: it is possible that an area first experiences strong erosion and then subsequent tsunami waves deposit the sediment in this eroded area (see, e.g., Li et al [2012a]), and thus the tsunami deposit thickness measured by geologists after an event records the information of sediment between the final bed elevation and the maximum erosion at the surveyed location (Fig. 5b). Therefore, it is not correct to compare the simulated thickness of a deposition region with the measured tsunami deposit thickness in the same region, and it is also incorrect to use the measured tsunami deposit thickness to indicate that this measured region is a tsunami deposition region.

Fig. 6 compares the deposit thicknesses surveyed in an inland area with those given by XBeach using the six formulas. For all the six computed results, high spikes can be observed in the region about 1000 m landward from the shoreline; this is the region where a sharp slope exists in the topography. The spikes were probably caused by the difference between the digitized and real topography in that region. All six formulas failed to produce results as good as those found in laboratory conditions, but the deposit thicknesses computed using different formulas are in order-of-magnitude agreement with the surveyed data. Apart from the spikes around 1,000 m from the shoreline, the results obtained using the formulas of Bagnold [1966], Van Rijn [1984a; b] and Engelund and Hansen [1967] agree better with the observations than the other four formulas do: the results computed using the formulas of Yang [1979] gave very large deposit thickness near shore and in the region between 1,000 and 2,000 m from the shoreline, while the formulas of Bijker [1967] and Ackers and White [1973] gave very large deposit thickness near the shoreline.

As we have pointed out that the measured deposit thicknesses cannot be used to infer the changes of bed profile, which is difficult to be derived from a post-tsunami survey, we show in Fig. 7 the changes of the bed profile obtained using the six formulas. In general, these formulas gave similar erosion and deposition patterns: severe erosion near the shoreline and sediment deposition (a large sandbar) in the offshore area. An exception is that for the formula of Yang [1979]: the formula of Yang [1979] predicted three large erosion regions (one wide region offshore, one medium erosion region onshore, one exceptionally large erosion region near the shoreline) and a very large offshore sandbar. The formulas of Engelund and Hansen [1967] and Bijker [1967] gave morphological changes

larger than the formulas of Bagnold [1966], Van Rijn[1984a; b]and Ackers and White [1973] did, and the formula of Ackers and White [1973] gave the smallest morphological changes among the six formulas. Our simulations (now shown here) showed that at high velocities, the formulas of Bijker [1967] and Engelund and Hansen [1967]gave equilibrium sediment concentration larger than other formulas did.

3.5. *Remarks on the six surveyed sediment transport formulas*

For real tsunamis, it seems that the formulas of Bagnold [1966] and Van Rijn[1984a; b] can give results more reasonable than do other formulas. For solitary waves or tsunami-like waves in laboratory conditions, the formulas of Bagnold [1966]and Van Rijn[1984a; b]and Ackers and White [1973] seem to give results in good agreement with the measured data. The formulas of Bijker [1967], Engelund and Hansen [1967] and Yang[1979]underestimated the erosion depth and the deposition thickness. In general, the formulas of Bagnold [1966]and Van Rijn[1984a; b] seem to give the most reliable results in both the field and laboratory conditions, possibly because these two formulas have been calibrated using a large set of field data: for the formula of Van Rijn[1984a; b], the water depths ranged from 1 m to 20 m and the averaged velocities ranged from 0.5m/s to 5 m/s (see Table 2); for the formula of Bagnold [1966], the water depths ranged from 0.22 m to 8.38 m and the averaged velocities ranged from 0.42m/s to 2.76 m/s (see Table 2) .In the next section, only the formula of Van Rijn[1984a; b]is employed when we use Delft3D to revisit the four cases discussed in this section.

4. Performances of XBeach and Delft3D

To see if Delft3D can give results better than XBeach, Delft3D was used to re-compute the four cases examined in section 3. In all the simulations in this section, Delft3D was run with 10 vertical sigma layers, which were specified as 2, 3, 4, 6, 8, 10, 12, 15, 20, 20% of the water depth (from the bottom to the surface).

Large tsunami waves always associated with high velocities and large bed shear stresses, resulting in high concentration of suspended sediment. Both the density stratification and hindered settling are the results of high SSC, and are considered in Delft3D: the density of the sediment-laden fluid ρ_{mix} is calculated by $\rho_{mix} = \rho_w + \sum c(1 - \rho_w / \rho_s)$ where ρ_w and ρ_s are the density of fluid and the density of sediment, and the settling velocity $w_s = (1 - c_s^{tot} / c_d)^5 w_{s,0}$ where c_s^{tot} is the total mass concentration of sediment in the water column and c_d is a reference density, assumed here to be 1600 kg/m³ (by see, e.g., Richardson and Zaki [1954]).

4.1. *Laboratory experiments*

For the three laboratory experiments listed in Table 3, the grid size was fixed at 0.1 m and the bottom roughness was parameterized using the Chezy coefficient with a fixed value of 65 m^{1/2}/s (for a flow depth of 0.03 m, this value of Chezy coefficient corresponds to a discrete roughness element of height 0.0002 m, which is about the diameter of sand used in the experiments). The model parameters used in Delft3D and XBeach are summarized in Table 4 for reference. When running Delft3D, the background horizontal diffusivity D_h^{back} and the background horizontal eddy viscosity ν_h^{back} were set to zero since it is not possible to assess the magnitudes of these two

parameters. In order to compare Delft3D and XBeach, both the horizontal diffusivity (D_h) and the horizontal eddy viscosity (ν_h) were set to zero when running XBeach.

For the case of Kobayashi and Lawrence [2004], the simulated bed profiles after running 4 and 8 solitary waves are compared with the experimental data in Fig. 8: both Delft3D and XBeach gave comparable erosion depths and deposition thicknesses, but Delft3D gave a wider deposition region since XBeach used a zero horizontal diffusivity but Delft3D used a non-zero horizontal diffusivity obtained by $k-\varepsilon$ model. For example, at the location 2.5 m offshore from the shoreline, Delft3D gave a maximum horizontal diffusivity of $0.015 \text{ m}^2/\text{s}$.

For the case of Young et al. [2010] with wave height $H=0.3\text{m}$, the coefficient of nonlinearity (wave-height/water-depth) was 0.3. A comparison between the results of XBeach and Delft3D is shown in Fig. 9. It can be seen that both XBeach and Delft3D significantly overestimated the erosion depth and deposition thickness. Again, Delft3D gave wider regions of deposition and erosion compared to XBeach.

For the case of Young et al. [2010] with wave height $H=0.6\text{m}$, the beach was exposed to multiple consecutive solitary waves of the same height $H=0.6 \text{ m}$. Fig. 10 compares the simulated bed profile changes after 3, 6 and 9 solitary waves with the measured data. For the deposition thickness and the width of the deposition region, Delft3D gave predictions better than XBeach for all the three cases in Fig. 10. Even though the computed erosion depth agreed reasonably well with the experiment after three waves, the difference between the measured and computed erosion depths increased with increasing number of attacking waves. As shown in Fig. 10, running XBeach with $\Delta x = 0.1\text{m}$ produced zigzag profiles in the erosion region for all the three cases. However, running XBeach with $\Delta x = 0.2\text{m}$ gave a smooth bed profile in the erosion region, as shown in Fig. 3.

4.2. Kuala Meurisi, Sumatra

Apotsos, et al. [2011b] studied this case using Delft3D with the formula of Van Rijn[1984a; b]. Negative deposit thicknesses can be found in the Figure 2 of Apotsos, et al. [2011b]. Since deposit thickness is always positive, it is suspected that Figure 2 in Apotsos, et al. [2011b] compared the measured deposit thickness with the computed change of bed elevation. We revisited this problem using Delft3D the formula of Van Rijn[1984a; b], but compared the measured deposit thicknesses from the field survey (Apotsos, et al. [2011b]) with those computed using XBeach and Delft3D with the model parameters listed in Table 4.

As did in Apotsos et al. [2011a], tsunamis waves were assumed to be normal to the shoreline and the wave form was digitized from Figure 3 in Apotsos et al. [2011a], as we did in Section 3.5. The grid size used in the simulation was 12 m in the cross-shore direction (since waves are normal to the shoreline and all the contour lines are parallel, XBeach is run as 1D model, Delft3D is run as a 2DV model). Following Apotsos et al. [2011a], bottom roughness was estimated from the White-Colebrook formulation using a Nikuradse roughness of 0.5m for the onshore region and 0.05m for the offshore region. As shown in Fig.11, both Delft3D (with both hindered settling and density stratification being considered) and XBeach gave comparable deposit thicknesses. The bed profiles obtained by Delft3D (with both hindering settlement and density stratification being considered) and XBeach are shown in Fig.

12. Compared to the bed profiles obtained by XBeach, Delft3D predicted a larger erosion depth in the shoreline area and a much thicker deposition thickness in the offshore area. However, in the inland area, both XBeach and Delft3D gave almost identical bed profiles.

5. Discussion on model parameters

Now we use XBeach and Delft3D to discuss the effects of bottom friction, horizontal eddy viscosity and diffusivity; in all the results given in this section, the other parameters were kept the same as we used in Section 4 (listed in Table 4) for each studied case. Only the formula of Van Rijn (1984a,b) will be used with XBeach and Delft3D in the following discussion.

5.1. Effect of bottom friction

Bottom friction plays an important role in determining the maximum run-up and this effect has been demonstrated by many previous studies [Liu *et al.*, 1995; Lynett *et al.*, 2002]: reducing bottom roughness will increase wave runup. It is expected that the computed flow velocities during the run-up and backwash flows are strongly affected by the distribution of bottom friction; as a result, the sediment transport process is also inevitably affected by the change in the flow velocity. To demonstrate the effect of bottom friction in both XBeach and Delft3D, the case studied in Section 3.4 and Section 4.2 was recomputed using XBeach and Delft3D with different values of bottom friction: (1) Nikuradse roughness $k_s = 0.002$ m in the offshore area and $k_s = 0.01$ m in the inland area; (2) a uniform $k_s = 0.002$ m in the computation domain; and (3) a uniform $k_s = 0.01$ m in the computation domain. The computed bed elevations using the three roughness configurations are compared in Fig. 13. For XBeach, the computed bed profiles onshore are close to each other, but the maximum deposition thickness computed with $k_s = 0.01$ m in the offshore area is only half of that with $k_s = 0.002$ m—a larger runup (and thus larger backwash velocity) due to a smaller bottom roughness may move more sand and result in a thicker offshore deposition. Compared to the results obtained using XBeach, much more severe erosion and a larger offshore deposition zone can be observed in the results of Delft3D.

It is also found from Fig. 13 that Delft3D is more sensitive to bottom roughness than XBeach is. A possible explanation for this is given here. Sediment transport rate is directly related to the bed shear stress. The bed shear stress in XBeach is calculated by a quadratic friction law using the depth-averaged horizontal velocity and a given bottom roughness (specified by either Chezy coefficient or Manning's roughness coefficient). The bed shear stress in Delft3D is related to the velocity in the layer immediately adjacent to the bottom, where both the turbulence intensity and the velocity (assumed to be logarithmic) are strongly affected by the bottom roughness (specified by Nikuradse's equivalent sand roughness, k_s , which has direct physical meaning). For a given Nikuradse's equivalent sand roughness k_s , both the Chezy coefficient and Manning's roughness coefficient vary with water depth, and thus is less sensitive to variation in k_s . As a result, the sediment transport is more sensitive to bottom roughness in Delft3D than in XBeach.

5.2. Effect of horizontal diffusivity

The horizontal diffusivity used in XBeach and Delft3D is related not only to turbulence motion, but also to additional processes such as numerical diffusion caused by coarse grids, discretization of differential equations, and dispersion introduced by depth-averaging [Rodi, 1984]. Therefore, the value of horizontal diffusivity is more of empirical nature and needs to be calibrated using available data.

Wave breaking can enhance turbulence intensity and horizontal diffusion, thus non-zero horizontal diffusivity should be used in XBeach and Delft3D. However, there is no available method for determining horizontal diffusivity. To assess the sensitivity of XBeach to the horizontal diffusivity, the experiment of Young et al (2010), discussed in Section 3.2, was recomputed with different values of diffusivity $D_h = 0, 0.01, 0.1, 1.0$, and the results are shown in Fig. 14. It can be seen that improvement over the results shown in Fig. 1 can be achieved with $D_h = 1.0$: a larger horizontal diffusivity helps spread the suspended sediment over a wider region offshore. We also recomputed this case using Delft3D with $D_h^{back} = 0.1 \text{ m}^2/\text{s}$ (the total horizontal diffusivity is not controlled by the background horizontal diffusivity since the maximum horizontal diffusivity given by $k-\varepsilon$ model is about $0.015 \text{ m}^2/\text{s}$). The numerical results show that the inclusion of a non-zero D_h^{back} produced much better results (figure is not included here).

5.3. Effect of horizontal eddy viscosity

In addition to energy dissipation due to bottom friction, processes such as wave breaking and vortex shedding from small objects or edges of large objects can also dissipate significant amounts of energy. To account for these types of energy dissipation, XBeach allows users to specify a horizontal eddy viscosity and Delft3D allows users to specify a background horizontal viscosity. As expected, large uncertainty may exist in the values of horizontal viscosity that users may use for a given problem.

To demonstrate the effects of horizontal eddy viscosity, the experiment of Young et al (2010) for $H=0.3\text{m}$ (discussed in Section 3.2) and the experiment of Young et al (2010) for $H=0.6\text{m}$ (discussed in Section 3.3) were recomputed using XBeach and Delft3D with a different value for the horizontal viscosity while keeping the horizontal diffusivity as zero. For the experiment of Young et al (2010) for $H=0.3\text{m}$, the results computed using $\nu_h = 0.1$ are shown in Fig. 15. Compared to Fig. 9, the increased horizontal viscosity reduced both the erosion depth and the deposition thickness; Delft3D with $\nu_h = 0.1$ produced a bed profile in good agreement with the measurement. Similarly, for the experiment of Young et al (2010) for $H=0.6\text{m}$, the results computed using $\nu_h = 0.02$ are shown in Fig. 16. For Delft3D $\nu_h = 0.02$, the increased horizontal viscosity reduced the computed erosion depths, giving computed bed profiles in good agreement with the measurements. For XBeach with $\nu_h = 0.02$, the improvement over the results in Fig. 10 is also obvious in both the deposition and erosion regions. It is concluded that the choice of a suitable ν_h for a chosen numerical model is a matter of model calibration rather than estimating turbulence intensity based on physical considerations. This is the typical drawback of these kinds of models in which the energy

dissipation due to wave breaking is handled mainly by numerical dissipation and thus the values of ν_h is affected by the grid size.

Integrating a wave breaking model with XBeach and Delft3D to account for the energy dissipation induced by breaking wave can be a way to overcome the drawback mentioned above. There are breaking models available for use with depth-averaged equations [Kennedy *et al.*, 2000; Madsen *et al.*, 1997; Zelt, 1991] These models contain trigger mechanisms to determine the onset and cessation of a breaking process, but some empirical parameters inherent in these models still need to be carefully calibrated [Zijlema and Stelling, 2008]. The eddy viscosity model proposed by Kennedy *et al.* [2000] has already been incorporated in the open-source tsunami simulation models such as COMCOT [Wang, 2009] and COULWAVE [Lynett and Liu, 2002], and good performance in modeling breaking wave run-up and rundown using shallow water equations and highly nonlinear Boussinesq equations has been shown [Lynett *et al.*, 2002]. It is desirable to incorporate breaking-wave models into XBeach and Delft3D to replace the user-defined horizontal eddy viscosity.

5.4. Effect of high suspended sediment concentration (SSC)

The high concentration of suspended sediment in water can result in fluid stratification and hinder the settling of sediment particles: the suspension time of a sediment particle can be greatly increased by the increased concentration of suspended sediment and fluid stratification can inhibit turbulent mixing (i.e., inhibiting the sediment in the lower layers from mixing all the way to the upper water column). The effect of high suspended sediment concentration on turbulent mixing is realized in Delft3D by a reduced mixing length: a smaller mixing length, calculated by using a turbulence model with the density of sediment-laden fluid, can lead to smaller vertical eddy diffusivity. In Delft3D, turbulent mixing and particle settling processes are not intertwined, and thus their effects can be discussed separately.

To understand the effects of density stratification and hindered settling, we use Delft3D to re-compute the case of Kuala Meurisi, Sumatra, using the data reported in Apotsos *et al.* [2011a]. The results obtained using different parameter settings are shown in Fig. 17. Snapshots of the computed SSC using the different parameter settings are shown in Fig. 18 for reference. The following observations can be made from Fig. 18 for the results given by Delft3D: (1) the depth-averaged SSC is not very sensitive to turbulent mixing (fluid stratification), even though the fluid stratification can slightly increase the depth-averaged SSC when the SSC is high; (2) hindered particle settling can greatly increase the depth-averaged SSC. Fig. 18(e) also reveals that the depth-averaged SSC given by XBeach is much lower even than that given by Delft3D without considering the effect of hindered settling. Thus, it is expected that the offshore deposition region given by XBeach is always narrower than that given by Delft3D (see Fig. 8, Fig. 9, Fig. 10, and Fig. 12).

When the SSC is low, the stratification effect can be basically ignored on sediment transport; this is also shown in Fig. 17, where the patterns of the erosion and deposition given by Delft3D with and without considering the stratification are more or less identical as long as the hindered settling is not considered. When the SSC is high, the stratification effect is expected to have a certain effect on sediment transport; this is also shown in Fig. 17, where the

location of the deposition region moved farther offshore after considering both density stratification and hindered settling. Since strong fluid stratification can inhibit sediment mixing from the lower layers with upper layers through turbulent mixing, the near-bottom SSC considering both density stratification and hindered settling would be larger than the one considering hindered settling effect only (see Fig. 18 (e)-(f)). The increased SSC due to density stratification would enhance hindered settling, increase the suspension time of a sediment particle, and thus increase the width of the offshore deposition region.

6. Conclusions

In this study, the performances of six widely-used sediment transport formulas were evaluated through these case studies and the capability of two open source model packages (XBeach and Delft3D) to simulate sediment transport induced by solitary waves or tsunami waves was also discussed. The benchmarks used in this study include three laboratory experiments and one field observations from a field survey after the 2004 Indian tsunami. Based on our numerical results, we draw the following conclusions:

1. All the six formulas surveyed failed to produce results in field conditions as good as in laboratory conditions. In general, the formula of Van Rijn[1984a; b] was found to yield relatively reliable results in both laboratory and field conditions. The formula of Bagnold [1966] could also give reasonable results.
2. XBeach and Delft3D can both predict satisfactory results in laboratory conditions with properly chosen model parameters. For real tsunamis, XBeach and Delft3D could give almost identical results when the SSC is low; however, XBeach would give a much narrower deposition region in the offshore area when the SSC is high due to the neglect of the density stratification and hindered settling effect.
3. Bottom roughness plays a crucial role in calculating the sediment transport rate. Delft3D was much more sensitive to the specification of spatial roughness distribution than XBeach.
4. Since the energy dissipation induced by the breaking waves is represented only by the numerical dissipation in both Delft3D and XBeach, thus the horizontal eddy viscosity becomes a calibration parameter that depends on grid size. It is therefore desirable to introduce wave breaking models in Delft3D and XBeach to remove the uncertainty in modeling energy loss due to wave breaking.

Acknowledgments

We are thankful to our colleagues Dr. Manuela Di Mauro and PHD candidate Sim Yisheng Shawn for their proofreading and helpful suggestions on this paper. We also would like to acknowledge Dr. Adam Switzer for his helpful comments. This work received the following financial supports: (1) the Open Research Fund Program of the State key Laboratory of Hydroscience and Engineering, Tsinghua University, China, through the project “Tsunami-induced scour around typical coastal trees” (No: sklhse-2011-B-04); and (2) the Earth Observatory of Singapore, Nanyang Technological University, Singapore, through the project “Tsunami Hazard Mitigation for West Sumatra”.

References

- Ackers, P., and W. R. White [1973] "Sediment transport: new approach and analysis" *Journal of Hydraulic Division*, 99(1), 2041-2060.
- Apotsos, A., G. Gelfenbaum, and B. Jaffe [2011a] "Process-based modeling of tsunami inundation and sediment transport" *Journal of Geophysical Research*, 116, 20.
- Apotsos, A., M. Buckley, G. Gelfenbaum, B. Jaffe, and D. Vatvani [2011b] "Nearshore Tsunami Inundation Model Validation: Toward Sediment Transport Applications" *Pure and Applied Geophysics*, 168(11), 2097-2119.
- Apotsos, A., G. Gelfenbaum, B. Jaffe, S. Watt, B. Peck, M. Buckley, and A. Stevens [2011c] "Tsunami inundation and sediment transport in a sediment-limited embayment on American Samoa" *Earth-Science Reviews*, 107(1-2), 1-11.
- Bagnold, R. A. [1966] "An approach to the sediment transport problem from general physics", paper presented at Geological Survey Professional Papers, Washington, USA.
- Bijker, E. W. [1967], Some considerations about scales for coastal models with movable bed. Delft Hydraulics Laboratory *Rep.*, Delft, The Netherlands.
- Deltares [2010], XBeach testbed report *Rep.*, Delft, The Netherlands.
- Deltares [2011], Delft3D-FLOW, User Manual, Simulation of multi-dimensional hydrodynamic flows and transport phenomena, including sediments *Rep.*, The Netherlands.
- Einstein, H. A. [1950] "The Bedload Function for Sediment Transportation in Open Channel Flows" *U.S. Department of Agriculture Soil Conservation Service Technical Bulletin no.1026*.
- Engelund, F., and E. Hansen [1967], A Monograph On Sediment Transport in Alluvial Streams *Rep.*, Teknisk Forlag, Copenhagen, Denmark.
- Galappatti, G., and C. B. Vreugdenhil [1985] "A depth-integrated model for suspended sediment transport" *Journal of Hydraulic Research*, 23, 359 - 377.
- Goto, C., Y. Ogawa, N. Shuto, and F. Imamura [1998], Numerical method of tsunami simulation with the leap-frog scheme *Rep.*, IUGG/IOC Time project, New York.
- Goto, K., and F. Imamura [2007] "Numerical models for sediment transport by tsunamis" *The Quaternary Research*, 46(6), 463-475.
- Goto, K., S. A. Chavanich, F. Imamura, P. Kunthasap, T. Matsui, K. Minoura, D. Sugawara, and H. Yanagisawa [2007] "Distribution, origin and transport process of boulders deposited by the 2004 Indian Ocean tsunami at Pakarang Cape, Thailand" *Sedimentary Geology*, 202(4), 821-837.
- Jaffe, B. E., and G. Gelfenbaum [2007] "A simple model for calculating tsunami flow speed from tsunami deposits" *Sedimentary Geology*, 200(3-4), 347-361.
- Jaffe, B. E., et al. [2006] "Northwest Sumatra and Offshore Islands Field Survey after the December 2004 Indian Ocean Tsunami" *Earthquake Spectra*, 22, 105-135.
- Kennedy, A. B., Q. Chen, J. T. Kirby, and R. A. Dalrymple [2000] "Boussinesq modeling of wave transformation, breaking, and runup. I: 1D" *Journal of Waterway, Port, Coastal and Ocean Engineering*, 126(1), 39-47.
- Kobayashi, N., and A. R. Lawrence [2004] "Cross-shore sediment transport under breaking solitary waves" *Journal of Geophysical Research C: Oceans*, 109(3).
- Lesser, G. R., J. A. Roelvink, J. A. T. M. v. Kester, and G. S. Stelling [2004] "Development and validation of a three-dimensional morphological model" *Coastal Engineering*, 51, 883-915.
- Li, L. L., Q. Qiu, and Z. H. Huang [2012a] "Numerical modeling of the morphological change in Lhok Nga, west Banda Aceh, during the 2004 Indian Ocean tsunami: understanding tsunami deposits using a forward modeling method" *Natural Hazards*, 1-26.
- Li, L. L., Z. H. Huang, Q. Qiu, D. H. Natawidjaja, and K. Sieh [2012b] "Tsunami-induced coastal change: scenario studies for Painan, West Sumatra, Indonesia" *Earth, Planets and Space*, 64, 1-18.
- Liu, L. F., H. Yeh, and C. Synolakis (Eds.) [2008] *Advanced Numerical Models for Simulating Tsunami Waves and Runup*, World Scientific, Singapore.
- Liu, P. L. F., C. Yong-Sik, M. J. Briggs, U. Kanoglu, and C. E. Synolakis [1995] "Runup of solitary waves on a circular island" *Journal of Fluid Mechanics*, 302, 259-285.
- Lynett, P., and L. F. Liu [2002], Modeling Wave Generation, Evolution, and Interaction with Depth-Integrated Dispersive Wave Equations COULWAVE Code Manual, Cornell University Long and Intermediate Wave Modeling Package *Rep.*
- Lynett, P. J., T. R. Wu, and P. L. F. Liu [2002] "Modeling wave runup with depth-integrated equations" *Coastal Engineering*, 46(2), 89-107.
- Madsen, P. A., O. R. Sørensen, and H. A. Schæffer [1997] "Surf zone dynamics simulated by a Boussinesq type model. Part II: surf beat and swash oscillations for wave groups and irregular waves" *Coastal Engineering*, 32(4), 289-319.
- Martin, M. E., R. Weiss, J. Bourgeois, T. K. Pinegina, H. Houston, and V. V. Titov [2008] "Combining constraints from tsunami modeling and sedimentology to untangle the 1969 Ozernoi and 1971 Kamchatskii tsunamis" *Geophysical Research Letters*, 35(1), L01610.
- McCall, R. T., J. S. M. Van Thiel de Vries, N. G. Plant, A. R. Van Dongeren, J. A. Roelvink, D. M. Thompson, and A. J. H. M. Reniers [2010] "Two-dimensional time dependent hurricane overwash and erosion modeling at Santa Rosa Island" *Coastal Engineering*, 57(7), 668-683.

- Megawati, K., F. Shaw, K. Sieh, Z. Huang, T. R. Wu, Y. Lin, S. K. Tan, and T. C. Pan [2009] "Tsunami hazard from the subduction megathrust of the South China Sea: Part I. Source characterization and the resulting tsunami" *Journal of Asian Earth Sciences*, 36(1), 13-20.
- Moore, A. L., B. G. McAdoo, and A. Ruffman [2007] "Landward fining from multiple sources in a sand sheet deposited by the 1929 Grand Banks tsunami, Newfoundland" *Sedimentary Geology*, 200(3-4), 336-346.
- Nakamura, T., N. Mizutani, and S. C. Yim [2009] "A three-dimensional coupled fluid-sediment interaction model with bed-load/suspended-load transport for scour analysis around a fixed structure" *Journal of Offshore Mechanics and Arctic Engineering*, 131(3), 1-9.
- Nelson, A. R., H. M. Kelsey, and R. C. Witter [2006] "Great earthquakes of variable magnitude at the Cascadia subduction zone" *Quaternary Research*, 65(3), 354-365.
- Nishihata, T., Y. Tajima, Y. Moriya, and T. Sekimoto [2006] "Topography change due to the Dec 2004 Indian Ocean Tsunami-Filed and numerical study at Kirinda port, Sri Lanka", paper presented at Proceedings of 30th International Conference on Coastal Engineering, ASCE.
- Paris, R., J. Fournier, E. Poizot, S. Etienne, J. Morin, F. Lavigne, and P. Wassmer [2010] "Boulder and fine sediment transport and deposition by the 2004 tsunami in Lhok Nga (western Banda Aceh, Sumatra, Indonesia): A coupled offshore-onshore model" *Marine Geology*, 268(1-4), 43-54.
- Pinegina, T. K., J. Bourgeois, L. I. L. I. Bazanova, I. V. Melekestsev, and O. A. Braitseva [2003] "A millennial-scale record of holocene tsunamis on the Kronotskiy Bay coast, Kamchatka, Russia" *Quaternary Research*, 59(1), 36-47.
- Richardson, J. F., and W. N. Zaki [1954] "Sedimentation and fluidization" *Transactions of the Institution of Chemical Engineers*, 32, 35-50.
- Rodi, W. [1984] Turbulence models and their application in hydraulics, State-of-the-art review, in *Paper presented by the IAHR-Section on Fundamentals of Division II: Experimental and Mathematical Fluid Dynamics*, edited, The Netherlands.
- Roelvink, D., A. Reniers, A. van Dongeren, J. van Thiel de Vries, R. McCall, and J. Lescinski [2009] "Modelling storm impacts on beaches, dunes and barrier islands" *Coastal Engineering*, 56(11-12), 1133-1152.
- Simpson, G., and S. Castellort [2006] "Coupled model of surface water flow, sediment transport and morphological evolution" *Computers & Geosciences*(32), 1600-1614.
- Spiske, M., R. Weiss, H. Bahlburg, J. Roskosch, and H. Amijaya [2010] "The TsuSedMod inversion model applied to the deposits of the 2004 Sumatra and 2006 Java tsunami and implications for estimating flow parameters of palaeo-tsunami" *Sedimentary Geology*, 224(1-4), 29-37.
- Sugawara, M., S. Ohkubo, and F. Imamura [2004] "Basic study on sand sedimentation by a tsunami on an uniform slope" *Tohoku Journal of natural Disaster Science*, 40, 265-270.
- Switzer, A. D., S. Srinivasalu, N. Thangadurai, and V. Ram Mohan [2012] Bedding structures in Indian tsunami deposits that provide clues to the dynamics of tsunami inundation, edited, pp. 61-77.
- Takahashi, T., N. Shuto, F. Imamura, and D. Asai [2000] "Modeling sediment transport due to tsunamis with exchange rate between bed load layer and suspended load layer.", paper presented at Proceedings of the International Conference on Coastal Engineering, ASCE.
- Titov, V. V., and C. E. Synolakis [1998] "Numerical modeling of tidal wave runup" *Journal of Waterway, Port, Coastal and Ocean Engineering*, 124(4), 157-171.
- Van Dongeren, A. R., and I. A. Svendsen [1997] "Absorbing-generating boundary condition for shallow water models" *Journal of Waterway, Port, Coastal and Ocean Engineering*, 123(6), 303-313.
- Van Rijn, L. C. [1984a] "Sediment transport: Part I: Bed load transport" *Journal of Hydraulic Division*, 110(10), 1431-1456.
- Van Rijn, L. C. [1984b] "Sediment transport: Part II: Suspended load transport" *Journal of hydraulic division*, 110(11), 1613-1641.
- Van Rijn, L. C. [1993] *Principles of sediment transport in rivers, estuaries and coastal seas.*, Aqua Publications, The Netherlands.
- van Rijn, L. C. [2007] "Unified view of sediment transport by currents and waves. II: Suspended transport" *Journal of Hydraulic Engineering*, 133(6), 668-689.
- Wang, X. [2009] User manual for Cornell multi-grid coupled tsunami model-COMCOT V1.7., edited, New Zealand.
- Xiao, H., Y. L. Young, and J. H. Prévost [2010] "Hydro- and morpho-dynamic modeling of breaking solitary waves over a fine sand beach. Part II: Numerical simulation" *Marine Geology*, 269(3-4), 119-131.
- Yang, C. T. [1979] "Unit Stream Power Equations for Total Load" *Journal of Hydrology*, 40, 123-138.
- Yang, C. T. [2003] *Sediment transport : theory and practice*, Krieger Pub.
- Yeh, H., L. F. Liu, and C. Synolakis (Eds.) [1996] *Long-Wave Runup Models*, World Scientific Singapore.
- Young, Y. L., H. Xiao, and T. Maddux [2010] "Hydro- and morpho-dynamic modeling of breaking solitary waves over a fine sand beach. Part I: Experimental study" *Marine Geology*, 269(3-4), 107-118.
- Zelt, J. A. [1991] "The run-up of nonbreaking and breaking solitary waves" *Coastal Engineering*, 15(3), 205-246.
- Zijlema, M., and G. S. Stelling [2008] "Efficient computation of surf zone waves using the nonlinear shallow water equations with non-hydrostatic pressure" *Coastal Engineering*, 55(10), 780-790.

List of tables

Table 1 Six formulas used in the paper

Table 2 Summary of the ranges of the key parameters in the data source used to validate the sediment transport formulas

Table 3 Basic parameters used in four cases

Table 4 Basic simulation parameters used in XBeach and Delft3D

Table 1 Six formulas used in the paper

Formula	Sediment transport formula	Notation
Van Rijn (1984)	$q_s = 0.012\bar{u} \frac{(\bar{u} - \bar{u}_{cr})^{2.4} d_{50} D_*^{-0.6}}{((s-1)gd_{50})^{1.2}}, \quad q_b = 0.005\bar{u}h \left(\frac{\bar{u} - \bar{u}_{cr}}{((s-1)gd_{50})^{0.5}} \right)^{2.4} \left(\frac{d_{50}}{h} \right)^{1.2}$	\bar{u} depth-averaged flow velocity (m/s) \bar{u}_{cr} critical depth-averaged flow velocity based on Shields (m/s) $\bar{u}_{cr} = 0.19(d_{50})^{0.1} \log(12h/3d_{90})$ for $0.0001m \leq d_{50} \leq 0.0005m$ $\bar{u}_{cr} = 8.50(d_{50})^{0.6} \log(12h/3d_{90})$ for $0.0005m \leq d_{50} \leq 0.002m$
Bagnold(1966)	$q_b = \frac{e_b}{(\rho_s - \rho)g(\tan\phi - \tan\beta)} \tau_b \bar{u}, \quad q_s = \frac{e_s(1-e_b)}{(\rho_s - \rho)g(w_s/\bar{u} - \tan\beta)} \tau_b \bar{u}$	ϕ - angle of repose of bed material β - angle of local of bottom slope $e_s \approx 0.2; e_b \approx 0.1$
Engelund-Hansen (1967)	$q_t = \frac{0.05\bar{u}^5}{(\rho_s/\rho - 1)^2 g^{0.5} d_{50} C^3}$	$C = 18 \log[(12h)/k_s]$, C : overall Chezy - coefficient
Ackers-White (1971, 1990)	$q_t = K\bar{u}d_{35} \left(\frac{\bar{u}}{u_*} \right)^n \left(\frac{Y - Y_{cr}}{Y_{cr}} \right)^m$ $Y = \left(\frac{u_*^n}{((s-1)gd_{35})^{0.5}} \right) \left(\frac{\bar{u}}{5.66 \log(10h/d_{35})} \right)^{1-n}, \quad D_* = d_{35} \left(\frac{(s-1)g}{\nu^2} \right)^{1/3}$	When $1 < D_* < 60$, $K = 10^{-3.46+2.79\log(D_*)-0.98(\log(D_*))^2}$, $m = 6.83/D_* + 1.67$ $n = 1 - 0.56 \log(D_*)$, $Y_{cr} = 0.23/D_*^{0.5} + 0.14$ When $D_* \geq 60$, $K = 0.025; m = 1.78; n = 0; Y_{cr} = 0.17$
Bijker(1971)	$q_b = bu_*d_{50}e^{-0.27/\mu\theta}, \quad q_s = 1.83q_b [I_2 + I_1 \ln(33h/k_s)]$ $I_1 = 0.216 \frac{A^{Z-1}}{(1-A)^Z} \int_A^1 \left(\frac{1-z}{z} \right)^Z dz, \quad I_2 = 0.216 \frac{A^{Z-1}}{(1-A)^Z} \int_A^1 \left(\frac{1-z}{z} \right)^Z \ln(z) dz$	$A = a/h$ - dimensionless reference level $z = z/h$ - dimensionless vertical coordinate $Z = w_s/(\kappa u_*)$ - suspension number, $b \approx 5$, $\mu = (C/C')$ C - overall Chezy coefficient C' - grain-related Chezy coefficient
Yang(1973)	$\log C_{is} = 5.435 - 0.286 \log \frac{\omega d}{\nu} - 0.457 \log \frac{u_*}{\omega}$ $+ \left(1.799 - 0.409 \log \frac{\omega d}{\nu} - 0.314 \log \frac{u_*}{\omega} \right) \log \left(\frac{\bar{u}S}{\omega} - \frac{u_*S}{\omega} \right), \quad q_t = 10^{-3} C_i \bar{u}h$, C_i is ft total load concentration in parts per million by weight	While the dimensionless critical velocity u_{cr}/ω is determined by $\frac{u_{cr}}{\omega} = \begin{cases} \frac{2.5}{\log(u_*d/\nu) - 0.06} + 0.66 & \text{for } 1.2 < \frac{u_*d}{\nu} < 70 \\ 2.05 & \text{for } 70 \leq \frac{u_*d}{\nu} \end{cases}$

Table 2 Summary of the ranges of the key parameters in the data source used to validate the sediment transport formula

No.	Sediment Transport Formula	Grain size range [mm]	Water depth range [m]	Velocity range [m/s]	Data type and no. of data sets
1	Bagnold [1966]	0.075-5	0.22-8.38	0.42-2.76	146 field data
2	Engelund and Hansen [1967]	0.19-0.93	-	-	100 sets of flume data*
3	Bijker [1967]	-	-	-	-
4	Ackers and White [1973]	0.2-0.61	0.18-7.17	-	925 sets of flume and field data*
5	Yang [1979]	0.063-2	-	-	463 sets of flume data [#]
6	Van Rijn [1984a; b]	0.1-2	1-20	0.5-5	Tested over a range of flume and field data*

*information is from Van Rijn [1993], [#] information is from Yang [2003]

Table 3 Basic parameters used in four cases

Case	Data source	Domain size [m]	D ₅₀ [mm]	h [m]	Beach Slope	Wave Type	H [m]	N	Δx [m]	C [m ^{1/2} /s]	v _h [m ² /s]	D _h [m ² /s]
1	Kobayashi and Lawrence (2004)	30.0×2.4	0.18	0.8	1:12	PSW ^(#)	0.216	8	0.2	65	0	1.0
2	Young et al (2010)	48.8×2.16	0.21	1	1:15	PSW	0.3	3	0.2	65	0.25	0.0
3	Young et al (2010)	48.8×2.16	0.21	1	1:15	PSW	0.6	9	0.2	65	0.02	0.0
4	Aptosos et al (2011a)	3996×10	0.5	-	variable	RTW*	~5	-	2	65	0	0

#: PSW=Positive Solitary Wave; *: RTW=Real Tsunami Wave

Table 4 Basic simulation parameters used in XBeach and Delft3D

Case	Data source	XBeach				Delft3D			
		Δx [m]	C/k _s [m ^{1/2} /s]	v _h [m ² /s]	D _h [m ² /s]	Δx [m]	C/k _s [m ^{1/2} /s]	D _h ^{back} [m ² /s]	V _h ^{back} [m ² /s]
1	Kobayashi and Lawrence (2004)	0.1	65	0	0	0.1	65	0	0
2	Young et al (2010)	0.1	65	0	0	0.1	65	0	0
3	Young et al (2010)	0.1	65	0	0	0.1	65	0	0
4	Aptosos et al (2011a)	12	0.5/0.05*	0	0	12	0.5/0.05*	0	0

*: The bottom roughness is specified by a Nikuradse roughness k_s estimated using the White-Colebrook formulation: 0.5m in the on-shore region and 0.05m in the offshore region.

List of figures

Fig. 1 The erosion and deposition simulated by six formulas (solid line) compared with Kobayashi's experimental data (dotted line) after 8 waves

Fig. 2 Bed elevation change simulated by six models (solid line) compared with Young's experimental data after 3 waves (dotted line)

Fig. 3 Bed elevation change simulated by six models (solid line) compared with Young's experimental data after 9 waves (dotted line)

Fig. 4 (a) Measured profile and (b) Water level predicted by a deep ocean propagation model used in Apotsos et al. (2011b)

Fig. 5 schematic for the explanation of (a) the thickness of a deposition region (bed elevation change includes the erosion depth and the thickness of a deposition region) and (b) deposit thickness

Fig. 6 Measured deposit thickness (dots) and predicted deposit thickness by six formulas (solid lines)

Fig. 7 Simulated erosion and deposition using six sediment formulas

Fig. 8 Bed profile changes after (a) 4 consecutive solitary waves and (b) 8 waves

Fig. 9 Bed elevation changes after 3 consecutive solitary waves with the parameter

Fig. 10 Bed elevation changes after 3, 6, 9 consecutive solitary waves attack in case (3)

Fig. 11 Measured deposit thickness and predicted deposit thickness by XBeach (solid line) and Delft3D (dashed line)

Fig. 12 The bed elevation change simulated by XBeach compared to the results by Delft3D considered both hindered settling effect and stratification effect.

Fig. 13 Bed elevation changes with different bottom roughness (a) 2D model; (b) 3D model

Fig. 14 Erosion and deposition after (a) 4 consecutive solitary waves and (b) 8 waves, with different horizontal diffusivities in XBeach

Fig. 15 Bed elevation changes after 3 consecutive solitary waves with the parameter $\nu_h = 0.1$, $D_h = 0$ in case (2)

Fig. 16 Bed elevation changes after 3, 6, 9 consecutive solitary waves with the parameter $\nu_h = 0.02$, $D_h = 0$ in case (3)

Fig. 17 Comparison of simulation results by Delft3D with or without hindered settling effect and stratification effect. (here Delft3D-hs-ds: both stratification and hindered settling effect are considered; Delft3D-hs: hindered settling effect only; Delft3D-ds: stratification only; Delft3D-none: neglect both effect;)

Fig. 18 Instantaneous snapshots of the sediment concentration (kg/m^3) during the backwash flow ($t \sim 50$ min) (a) both stratification and hindered settling effect are considered; (b) hindered settling effect only; (c) stratification only; (d) neglect both effect; (e) comparison of the calculated depth-averaged sediment concentration by XBeach and Delft3D; (f) comparison of vertical SSC distribution at locations of $x = -500$ m, -1120 m, -1440 m with hindered settling effect only and both stratification and hindered settling effect.

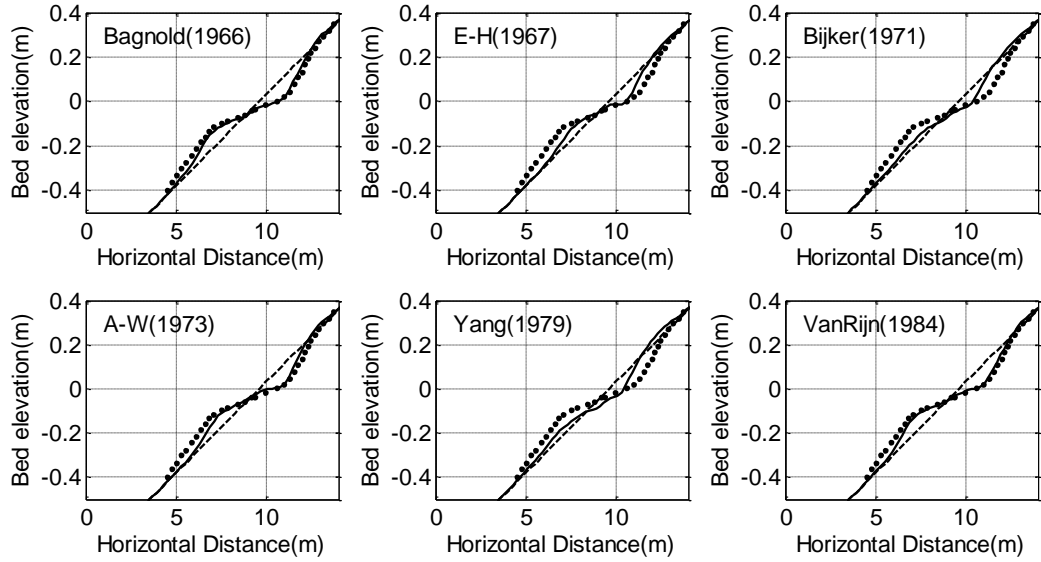


Fig. 1 The erosion and deposition simulated by six formulas (solid line) compared with Kobayashi's experimental data (dotted line) after 8 waves

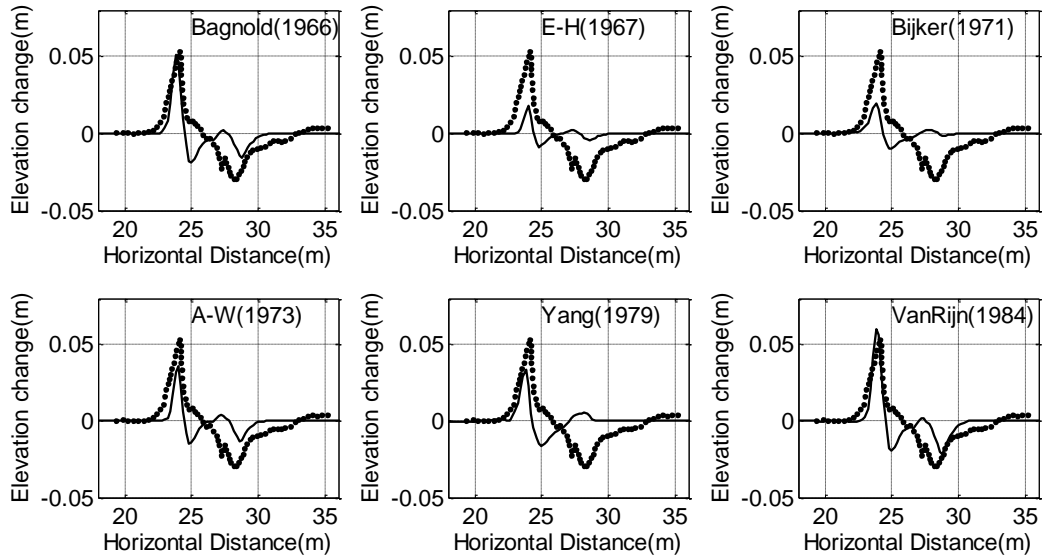


Fig. 2 Bed elevation change simulated by six models (solid line) compared with Young's experimental data after 3 waves (dotted line)

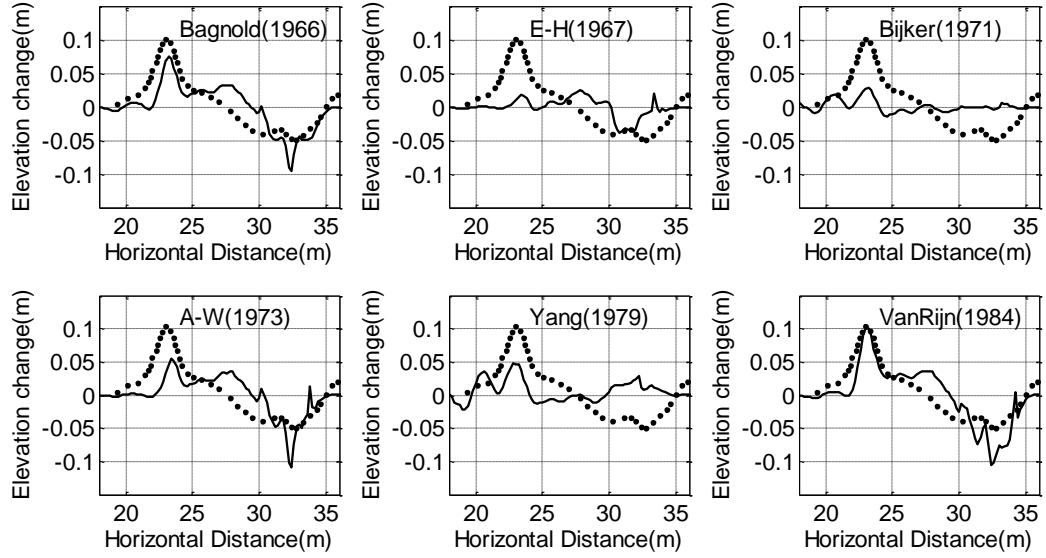


Fig. 3 Bed elevation change simulated by six models (solid line) compared with Young's experimental data after 9 waves (dotted line)

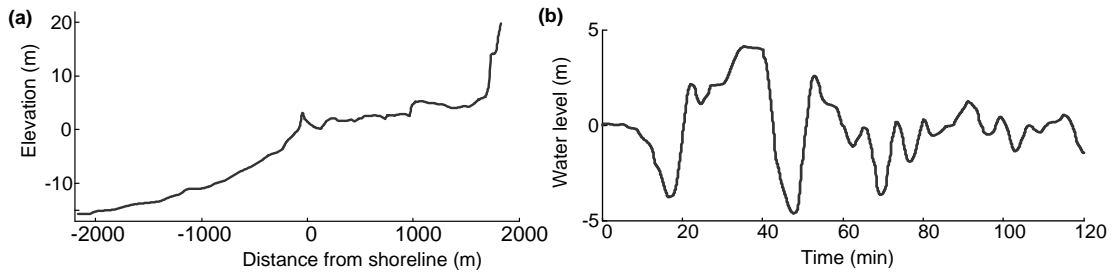


Fig. 4 (a) Measured profile and (b) Water level predicted by a deep ocean propagation model used in Apotsos et al. [2011a]

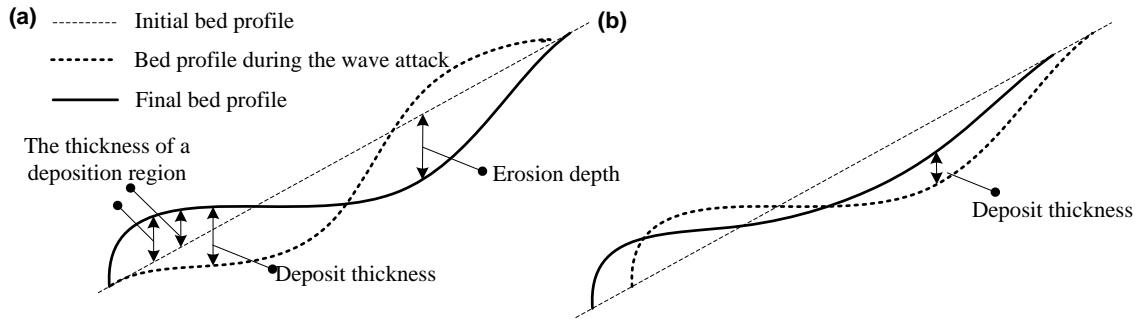


Fig. 5 schematic for the explanation of (a) the thickness of a deposition region (bed elevation change includes the erosion depth and the thickness of a deposition region) and (b) deposit thickness

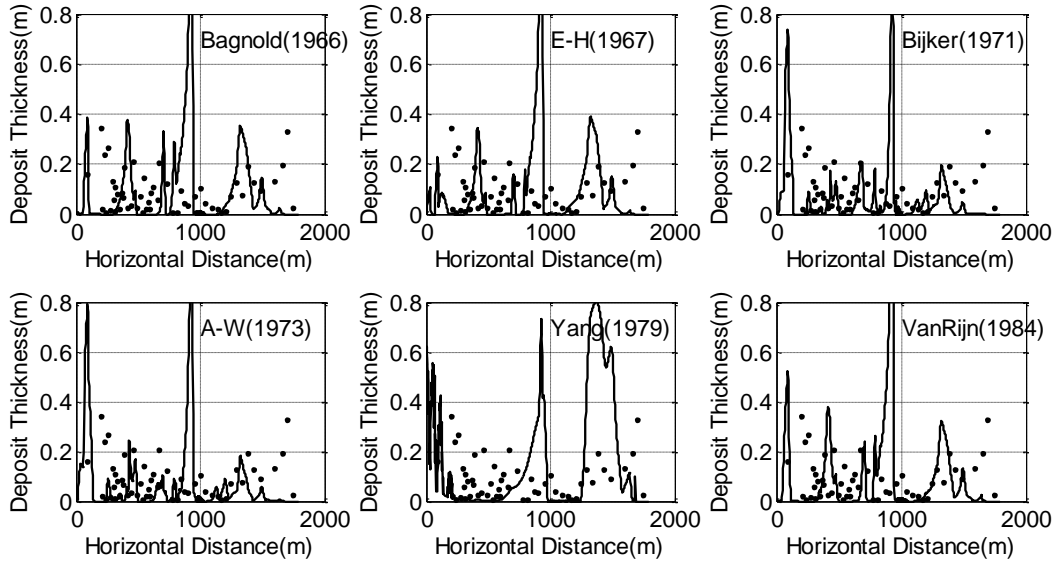


Fig. 6 Measured deposit thickness (dots) and predicted deposit thickness by six formulas (solid lines)

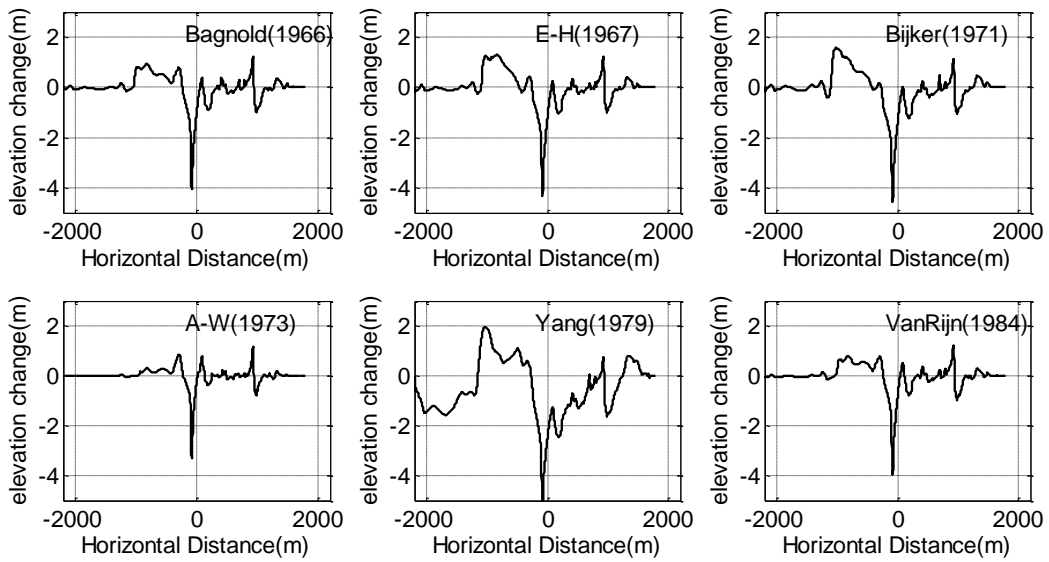


Fig. 7 Simulated erosion and deposition using six sediment formulas

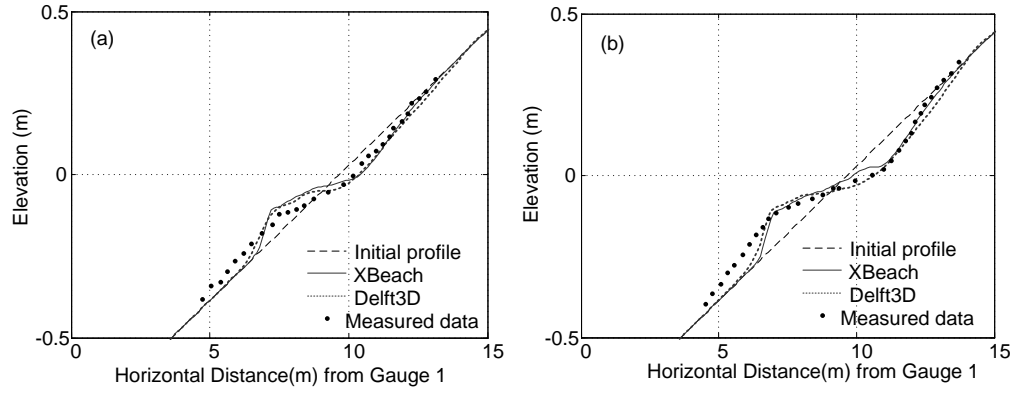


Fig. 8 Bed profile changes after (a) 4 consecutive solitary waves and (b) 8 waves (Gauge 1 located at the toe of the sand beach)

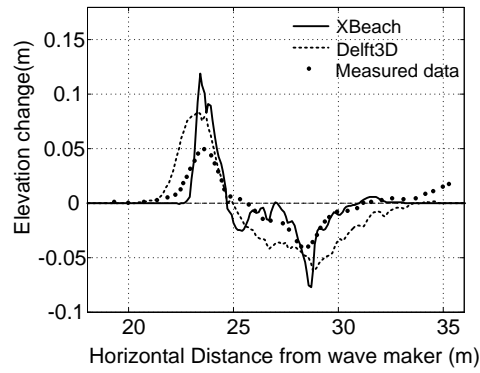


Fig. 9 Bed elevation changes after 3 consecutive solitary waves

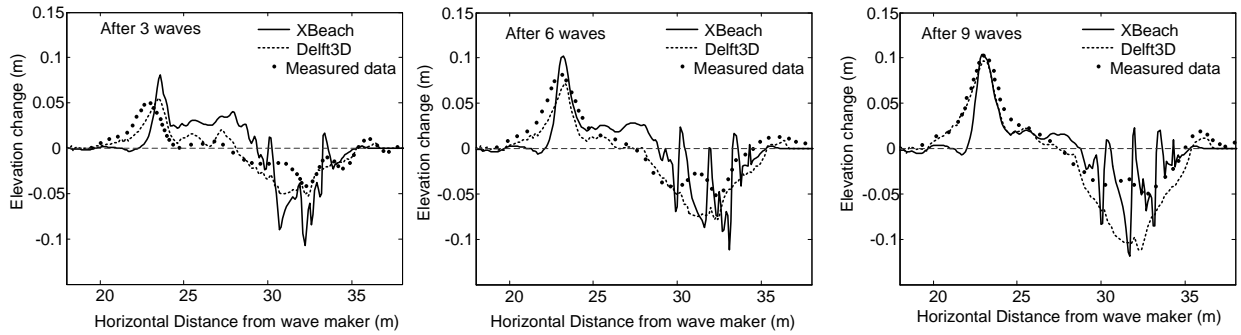


Fig. 10 Bed elevation changes after 3, 6, 9 consecutive solitary waves attack in case (3)

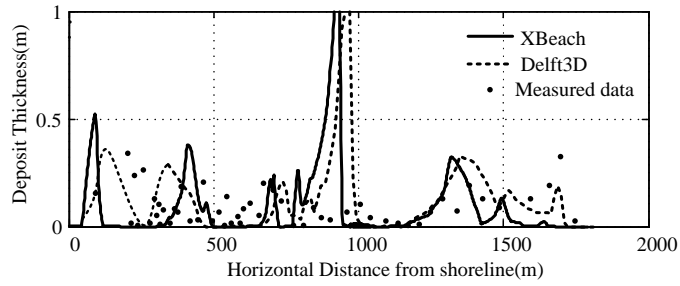


Fig. 11 Measured deposit thickness and predicted deposit thickness by XBeach (solid line) and Delft3D (dashed line)

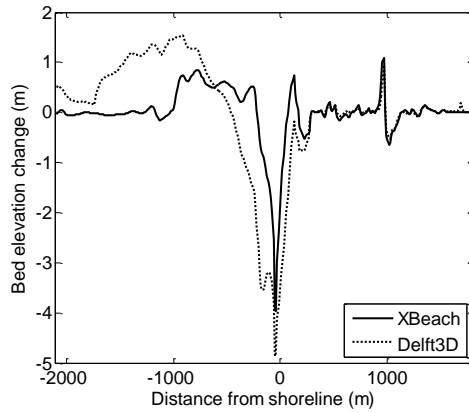


Fig. 12 The bed elevation change simulated by XBeach compared to the results by Delft3D considered both hindered settling effect and stratification effect.

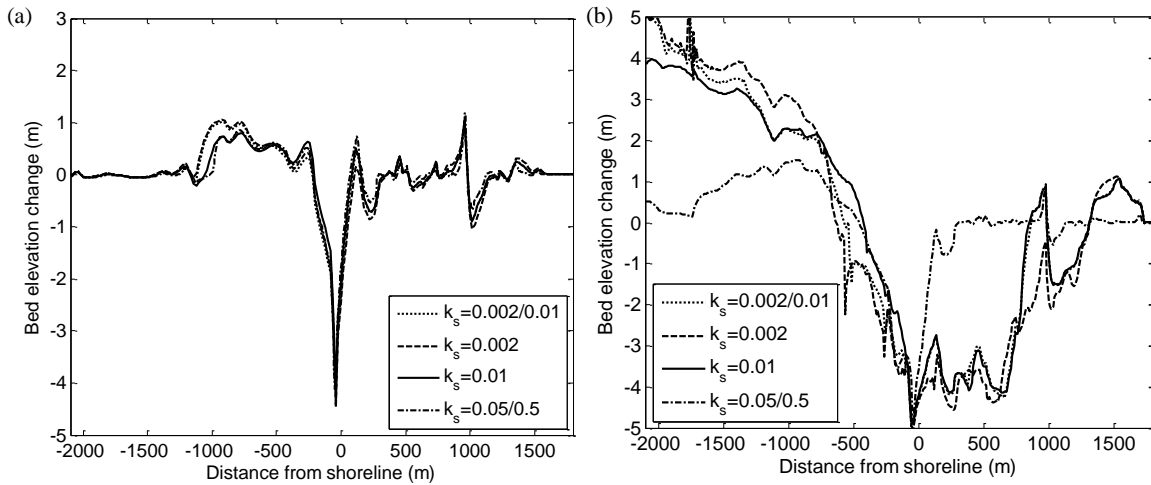


Fig. 13 Bed elevation changes with different bottom roughness (a) XBeach; (b) Delft3D

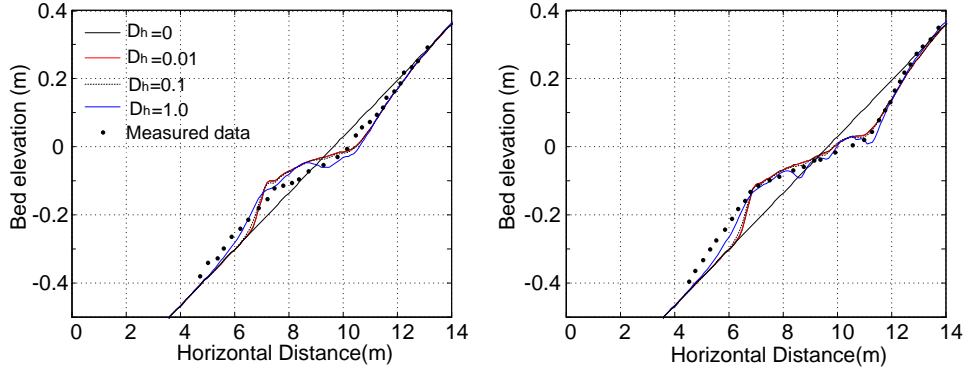


Fig. 14 Erosion and deposition after (a) 4 consecutive solitary waves and (b) 8 waves, with different horizontal diffusivities in XBeach

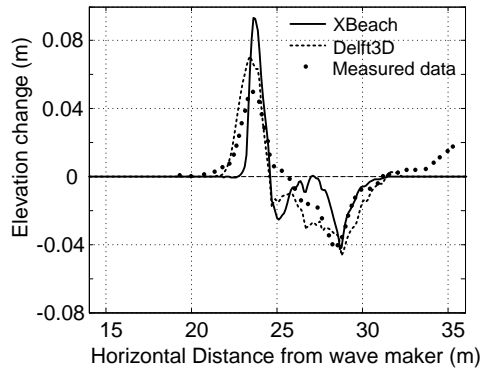


Fig. 15 Bed elevation changes after 3 consecutive solitary waves with the parameter $\nu_h = 0.1, D_h = 0$ in case (2)

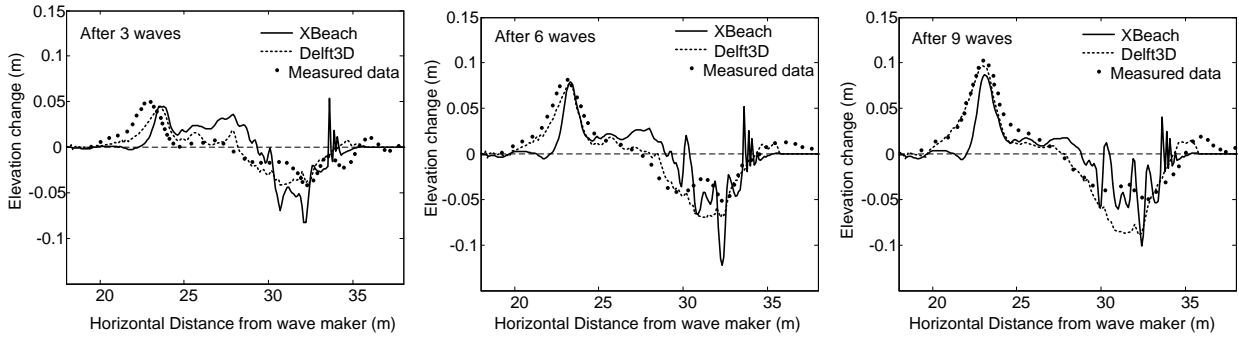


Fig. 16 Bed elevation changes after 3, 6, 9 consecutive solitary waves with the parameter $\nu_h = 0.02, D_h = 0$ in case (3)

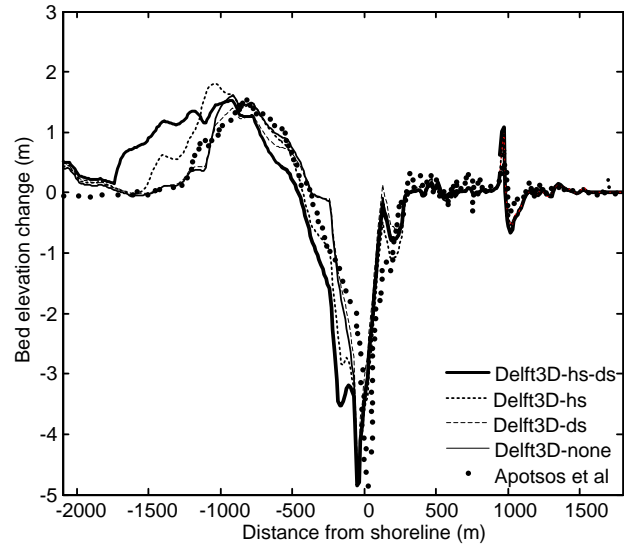


Fig. 17 Comparison of simulation results by Delft3D with or without hindered settling effect and stratification effect. (here Delft3D-hs-ds: both stratification and hindered settling effect are considered; Delft3D-hs: hindered settling effect only; Delft3D-ds: stratification only; Delft3D-none: neglect both effect;)

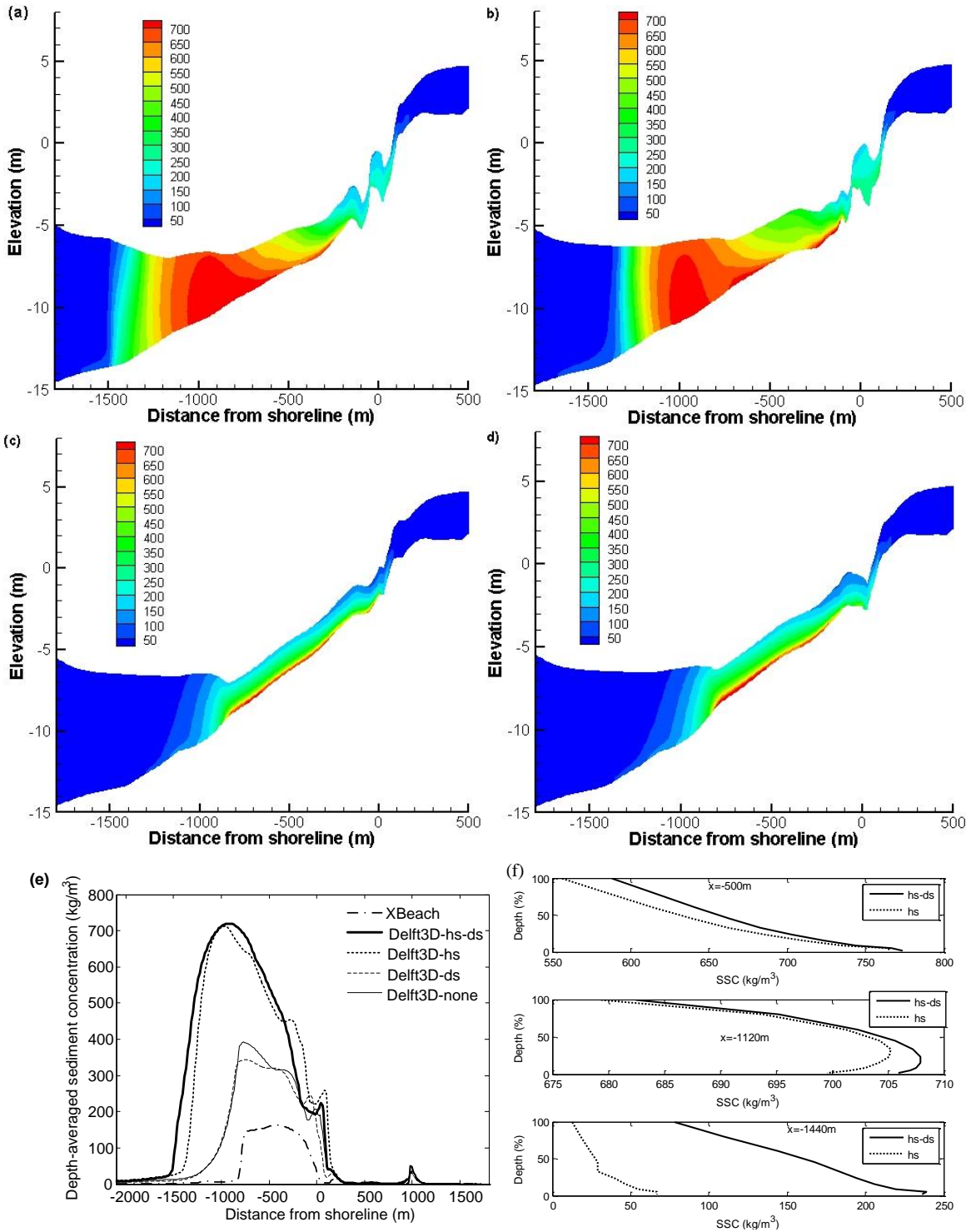


Fig. 18 Instantaneous snapshots of the sediment concentration (kg/m^3) during the backwash flow ($t \sim 50$ min) (a) both stratification and hindered settling effect are considered; (b) hindered settling effect only; (c) stratification only; (d) neglect both effect; (e) comparison of the calculated depth-averaged sediment concentration by XBeach and Delft3D; (f) comparison of vertical SSC distribution at locations of $x = -500\text{m}$, -1120m , -1440m with hindered settling effect only and both stratification and hindered settling effect.